# Cloud Parameters and Temperature Profile Retrieval from Infrared Sounder Data

HWA-YOUNG M. YEH,* AND THOMAS H. VONDER HAAR

*Cooperative Institute for Research in the Atmosphere, Colorado State University, Fort Collins, CO 80523*

KUO-NAN LIOU

*Department of Meteorology, University of Utah, Salt Lake City, UT 84112*

(Manuscript received 25 March 1985, in final form 14 June 1985)

ABSTRACT

An inversion method is applied to the remote sensing of atmospheric temperature profiles in the presence of clouds. The method simultaneously calculates cloud-top pressure, amount, and spectral emissivity, along with the temperature profile retrieval. Numerical analyses and retrieval experiments are carried out by using simulated sounder data. The sensitivity of the computed radiances to measurement noise and numerical errors is also examined. The retrieval results are physically discussed and numerically compared with the model atmospheric profiles. Comparisons reveal that the noise effect is more pronounced for thinner and/or smaller fractional cloud cases. It is also noted that the cloud thickness variation has a slight effect on temperature retrieval. Experiments on the proposed algorithm are carried out utilizing the High Resolution Infrared Sounder (HIRS) data of NOAA-6 and TIROS-N. Although the results of the experiments are difficult to verify quantitatively, the retrieved cloud cover and temperature field at 500 and 700 mb compare reasonably well with the synoptic reports and GOES satellite images.

## 1. Introduction

Although the nonuniqueness of the inversion problem using infrared radiances sensed by satellites introduces difficulties into the determination of atmospheric composition, numerical recovery of the temperature profile in recent years has proven to be somewhat successful. Accurate temperature profiles for clear atmospheric conditions have been derived (e.g., see Chahine, 1970; Smith, 1970). In addition, numerical procedures utilizing two adjacent fields of view for the recovery of temperature profiles in cloudy atmospheres have been proposed by Smith *et al.* (1979) and Chahine (1974). Hillger and Vonder Haar (1977, 1981) have demonstrated the feasibility of deriving mesoscale temperature and moisture fields from satellite infrared channels by using a simple cloud correction technique. All of these investigations, however, have assumed that clouds are blackbodies in the retrieval analyses. There are circumstances in which the specific treatment of nonblack clouds is required. For instance, the cloud emissivity of cirrus clouds remains less than unity even when their thickness exceeds several kilometers, while the emissivity of stratocumulus may never reach unity (e.g., Hunt, 1973). It has been noted by numerous researchers that the presence of cirrus or other nonblack clouds introduces serious difficulties into the retrieval of temperature and humidity profiles and surface conditions.

Cirrus clouds are global in nature, occupying the upper troposphere and occasionally extending to the lower stratosphere. In an application of infrared radiance data for day and night mapping of the global distribution of the horizontal cloud cover and the corresponding cloud top pressure level, Chahine (1982) found that the effective cloud cover derived from 15 $\mu$m data is about 25% less than that obtained from visible data. It has been suggested that this discrepancy may be partly due to the existence of cirrus or other nonblack clouds in the atmosphere (e.g., Susskind *et al.*, 1984). In this paper we wish to explore the theoretical foundation and numerical technique for the determination of the temperature profile and cloud properties under any cloudy conditions.

In the following sections, we present the basic formulation of the upwelling radiance and relaxation method for the retrieval of cloud-top pressure, emissivity, amount, and temperature profile in cloudy atmospheres. Numerical experiments and a number of case studies utilizing the NOAA-6 and TIROS-N High Resolution Infrared Sounder (HIRS/2) data for the retrieval are then described and discussed physically.

## 2. Theoretical background

Consider an atmosphere containing a fractional cloud cover $A$ within a satellite instantaneous field-of-

* Present affiliation: SASC Technologies, Inc., Hyattsville, MD 20784.

view (IFOV). The emitted radiation intercepted by the satellite radiometer can be written in an equation for the upwelling radiance at the top of the atmosphere (Yeh, 1984):

$$\tilde{I}(\nu_j) = I(\nu_j) - A[1 - \tau_c(\nu_j)]I'(\nu_j, P_c), \quad (1)$$

where

$$I'(\nu_j, P_c) = B[\nu_j, T(P_s)]\tau(\nu_j, P_s) - B(\nu_j, P_c)\tau(\nu_j, P_c) + \int_{P_s}^{P_c} B[\nu_j, T(P)]K(\nu_j, P)d(\ln P), \quad (2)$$

and $\nu_j$ denotes the wavenumber ($cm^{-1}$) of the spectral channel, $B$ is the spectral Planck function associated with temperature $T$, $\tau$ the atmospheric transmission function between the satellite sensor and the pressure level $P$, $\tau_c$ the cloud transmissivity, $P_s$ and $P_c$ indicate the surface and cloud top pressures respectively, and $K(\nu_j, P) = d\tau(\nu_j, P)/d(\ln P)$ is the spectral weighting function. In Eq. (1), the two terms on the right-hand side represent, respectively, the clear sky radiance $I(\nu_j)$ and the correction of the first term due to cloud contamination within the IFOV. Note that in writing the preceding equations, one assumes that the surface emissivity is unity and that the cloud reflectivity is negligible.

In the following subsections, the theoretical bases for the cloud properties and temperature retrieval are outlined.

### *a. Determination of cloud top pressure*

The method adopted here for the cloud top pressure calculation is a modification of the technique described in detail by Yeh and Liou (1983). There are two important approximations in this method: 1) the cloud transmissivity is considered to be independent of the channel number within the 15 $\mu$m $CO_2$ absorption band; and 2) the weighting function in Eq. (2) is only slightly dependent on temperature and moisture profiles. We define a function $H$ by taking the ratio of the differences between clear sky and satellite measured radiances in two adjacent channels. Because the fractional cloud effect on both channels is eliminated during the process of taking the ratio, we find that the $H$ function has the same form as that defined by Yeh and Liou [Eq. (12), 1983]. The clear sky radiance can be calculated by utilizing climatological profiles, which are also used as initial guesses in the iteration to be discussed below. In the previous study, the function $H$ proved to be relatively insensitive to the temperature profile variation and generally had a monotonic relation to the cloud top pressure in the troposphere. Since the function $H$ can be directly computed from the satellite measured radiances, the cloud top pressure can then be uniquely determined. More detailed discussions of this method can also be found in Wielicki and Coakley (1981) and McCleese and Wilson (1976).

### *b. Determination of cloud amount and emissivity*

Recently, the application of dual channel radiances at 13.4 and 11 $\mu$m of the HIRS/2 to the cloud amount and emissivity retrieval was carried out by Yeh (1984). Since the radiances measured by both channels are primarily contributed from the gaseous emission in the lower atmosphere and the surface in clear conditions, and in view of the weighting function depicted in Fig. 1, they are extremely sensitive to the presence of clouds at any altitude. For nonblack clouds, the cloud radiative properties at these two frequencies are distinct. A fairly constant relationship may be established between the mass absorption coefficients of these two channels. Thus, we may form an equation, based on two sets of radiance information and two unknowns, which may be solved by an interactive scheme. Such an equation may be written (Yeh, 1984)

$$f\chi - g\chi^r - (f - g) = 0 \quad (3)$$

where

$$\left.\begin{aligned} f &= [I(\nu_7) - \tilde{I}(\nu_7)]I'(\nu_8, P_c) \\ g &= [I(\nu_8) - \tilde{I}(\nu_8)]I'(\nu_7, P_c) \\ \chi &= \tau_c(\nu_8) \\ \chi^r &= \tau_c(\nu_7) \end{aligned}\right\}. \quad (4)$$

The subscripts 7 (13.4 $\mu$m) and 8 (11 $\mu$m) in the equations denote the channel numbers of the HIRS/2, and $r = K_{13.4\,\mu m}/K_{11\,\mu m}$, where $K$ is the mass absorption coefficient. Paltridge and Platt (1976) found that $K$ is approximately constant for the spectrum between 8 to 14 $\mu$m within a given cloud type. The value of $r$ is about 1.1, derived from the experiments conducted by Feddes and Liou (1978) for both ice and water clouds. However, it should be noted that those findings are based on only a few measurements and calculations. More study is necessary, especially in the case with

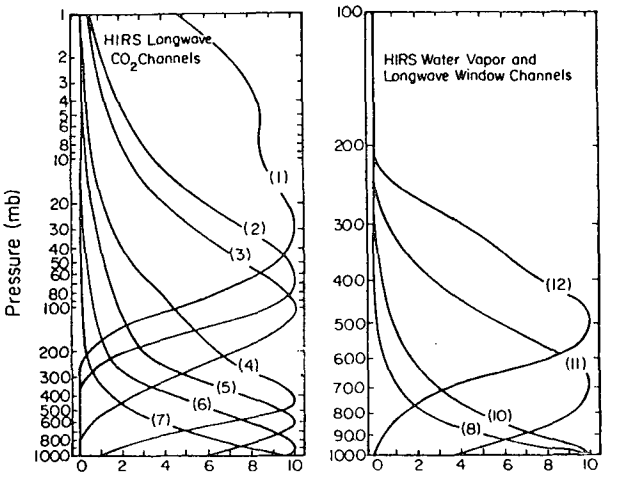


FIG. 1. Weighting functions of the HIRS/2 15 $\mu$m $CO_2$, 6.7 $\mu$m $H_2O$ and window channels.

nonspherical ice crystals and in the typical situation where particles within the cloud are large (radii $> 50$ $\mu$m).

Since the cloud reflection is ignored, the cloud emissivity in the 11 $\mu$m spectral region is then equal to $(1 - \chi)$, and the fractional cloud cover is

$$A = [I(\nu_8) - \tilde{I}(\nu_8)]/[(1 - \chi)I'(\nu_8, P_c)]. \quad (5)$$

In solving these equations, we need some empirical justification for the cases when relatively thin clouds and/or small cloud fractional cover are present in an IFOV. This is because the level of measurement noise is usually more noticeable from weak signals due to the presence of clouds (Yeh, 1984).

### c. *Reconstruction of clear sky radiances and temperature profile retrieval*

In the reconstruction of clear sky radiances, we first define the effective cloud emissivity, which will frequently be used in the next section when the convergent conditions for the iteration are discussed, as follows

$$\epsilon_c(\nu_j) = A[1 - \tau_c(\nu_j)]. \quad (6)$$

The clear sky radiance can thus be estimated by knowing $\tau_c$ in the 15 $\mu$m $CO_2$ spectral region from the following expression

$$I(\nu_j) = \tilde{I}(\nu_j) + \epsilon_c(\nu_j)I'(\nu_j, P_c). \quad (7)$$

Using the definition of cloud transmissivity, we may express $\tau_c$ as an exponential function of the product of the mass absorption coefficient $K$ and the water path length $w$ (Liou, 1980). Note that $K_{13.4\,\mu m}$ may be related to $K_{11'\mu m}$ by a fairly constant parameter $r$, regardless of the cloud types. If we assume that the cloud transmissivity varies slightly for channels within the HIRS/2 15 $\mu$m $CO_2$ absorption band, we may obtain

$$\tau_c(\nu_j) = [\tau_c(\nu_8)]^r, \quad j = 1, \ldots, J \quad (8)$$

where $J$ is the total number of channels within the 15 $\mu$m spectral region.

Once the clear sky radiance is reconstructed, we may employ a shape-preserving interpolation formula proposed by Chahine (1974, 1975) for the temperature profile retrieval. For clarity, we use $n$ to indicate the $n$th "outer" iteration which includes retrievals of cloud parameters and the temperature profile, and $m$ to denote the $m$th "inner" iteration for temperature profile retrieval based on the clear sky radiance $I^n(\nu_j)$. We can estimate $I^n(\nu_j)$ from Eq. (7) by using $\epsilon_c{}^n(\nu_j)$ and $P_c{}^n$ and $I^{n'}$. The temperatures $T^n_m(P)$ are computed for the pressure levels where the weighting functions have their peaks. At any of these pressure levels, we obtain a value of the Planck radiance for the next iteration $m + 1$ as follows:

$$B[\nu_j, T^n_{m+1}(P_j)] = B[\nu_j, T^n_m(P_j)]I^n(\nu_j)/I^n_m(\nu_j), \quad j = 1, \ldots, J \quad (9)$$

where $P_j$ is the pressure level at which the curve $K(\nu_j, P)$ has its maximum, and $I^n_m(\nu_j)$ is the outgoing radiance at the $m$th iteration and can be written,

$$I^n_m(\nu_j) = B[\nu_j, T^n_m(P_s)]\tau(\nu_j, P_s) + \int_{P_s}^{0} B[\nu_j, T^n_m(P)]K(\nu_j, P)d(\ln P). \quad (10)$$

At the maximum weighting function level of each channel, a temperature $T^n_{m+1}(P_j)$ is computed from $B[\nu_j, T^n_{m+1}(P_j)]$ with an inverse process. Since the Planck function can be expressed as

$$B[\nu_j, T(P)] = a\nu_j{}^3/[\exp(b\nu_j/T) - 1], \quad (11)$$

we may write the relaxation transformation in the form,

$$T^n_{m+1}(P_j) = \alpha^n_m(P_j)T^n_m(P_j), \quad (12)$$

where $\alpha^n_m(P_j)$ are scaling factors which may be obtained by substituting Eq. (11) into Eq. (9). In Eq. (11), $a$ and $b$ are two constants with $a = 1.19106 \times 10^{-5}$ erg s$^{-1}$ cm$^{-1}$ and $b = 1.4388$ cm deg, respectively.

In the iteration of Eqs. (9), (10), and (12), if the convergence criterion is not satisfied within five iterations, a slower iteration scheme, which smooths out random noise by applying weights to the scaling factors, is then used. The iteration process of each channel should be terminated when its iterative residual approaches an asymptotic value. Based on this process, the final solution depends on the initial guess by preserving the form of the input temperature profile in the steps of the iterative solution.

## 3. Numerical experiment

### a. *Numerical procedures*

As discussed previously, the cloud top pressure calculation is not strongly dependent on the atmospheric profile up to the tropopause. Therefore, in practice, the cloud top pressure may be determined by an initial guess of the temperature profile prior to the numerical iteration, to be discussed later. In the computation of the cloud amount and emissivity [Eqs. (3), (4) and (5)], an initial guess or the iteratively retrieved temperature profiles will be used as input data for estimating the thermal gaseous emission from the atmosphere. In turn, the resultant cloud parameters will be employed in the reconstruction of clear sky radiances, from which the retrieval of temperature profiles will be carried out. The detailed numerical procedures for the algorithm are described as follows:

(i) Choose an initial temperature profile $T^\circ(P)$. The cloud top pressure can immediately be determined by the ratio method as described in Section 2a. It would be advantageous to have, as an initial guess, a climatological profile not only adjusted to seasonal change, but also to local time variations over the area of interest. The local time adjustment is particularly important

for some areas, such as the tropics where the diurnal temperature variation may be more significant than the seasonal changes, or over continents where an early morning temperature inversion is usually a persistent feature.

(ii) Calculate the cloud emissivity and amount based on the measured satellite radiances and the temperature profile of either the initial guess or the previous iteration, as described in Section 2b.

(iii) If the residual of the effective cloud emissivity,

$$\Delta\epsilon_c^n(\nu_j) = |\epsilon_c^{n+1}(\nu_j) - \epsilon_n^n(\nu_j)| \tag{13}$$

is within a previously imposed criterion, say, $1 \times 10^{-3}$, then $A^{n+1}$ and $\tau_c^{n+1}$ are the approximate solutions, and the entire iteration stops after step 4 is accomplished. Otherwise, continue the iterations.

(iv) Reconstruct clear sky radiance by Eq. (7), then execute the temperature profile retrieval by the shape-preserving method.

1) Use the climatological or the last iterative profiles as an initial guess ($m = 0$) for $T_m^n(P)$.

2) Substitute $T_m^n(P)$ into Eq. (10) and compute the outgoing radiances $I_m^n(\nu_j)$ for all $J$ sounding frequencies.

3) Obtain the next iteration $T_{m+1}^n(P_j)$ from the relaxation equation (9).

4) Go back to step 2 and repeat it until the computed radiances $I_m^n(\nu_j)$ agree with $I^n(\nu_j)$. If the rms residuals

$$R^n(\nu_j) = \left\{\frac{1}{J}\sum_{j=1}^{J}[I^n(\nu_j) - I_m^n(\nu_j)]^2\right\}^{1/2} \tag{14}$$

approach an asymptotic value, $T_m^n(P)$ is a solution.

(v) Go back to (ii) until the condition described in step (iii) is satisfied.

In order to test the validity of the foregoing iterative steps, we shall construct a hypothetical cloudy atmosphere and perform numerical calculations to obtain the necessary parameters. The sensitivity of the numerical procedures to measurement noise will be examined, and subsequently, the bias and stability of this algorithm will be analyzed.

### b. *Convergence of the iterations*

Since the convergence conditions of temperature profile retrieval in a clear atmosphere [step 4 in (iv)] have been discussed by Barcilon (1975), we shall concentrate on the convergence property of "outer" iterations including steps (ii)–(v), in this study.

It is a good approximation that the given gaseous absorption above 800 mb in the atmosphere can be neglected for spectral channels in the 11 $\mu$m window region, in view of its weighting function (Fig. 1). Therefore, from Eqs. (1) and (6) we can derive the effective cloud emissivity $\epsilon_c(\nu_8)$ in a different form,

$$\epsilon_c(\nu_8) = \frac{I(\nu_8) - \tilde{I}(\nu_8)}{I(\nu_8) - B[\nu_8, T(P_c)]}. \tag{15}$$

In the following discussion, we shall prove the convergence of the proposed iterative scheme.

*Theorem:* Given $I^n(\nu_8) \to I(\nu_8)$, then the iterations (ii)–(iv) will converge to the solution of Eq. (1).

*Proof:* Let us begin the proof by stating its final objective. If we can prove that

$$|\epsilon_c^{n+1}(\nu_8) - \epsilon_c(\nu_8)| \leqslant |\epsilon_c^n(\nu_8) - \epsilon_c(\nu_8)| \tag{16}$$

then the convergence of iterations [steps (ii) to (v)] is valid, provided that the convergence of the temperature profile retrieval for a clear atmosphere [step (iv)] is satisfied.

For convenience, we write $B[\nu_j, T^n(P_c)]$ as $B_j^n(P_c)$ in the following derivation. From Eq. (15), we may obtain $\epsilon^{n+1}$ with $I$ replaced by $I^n$ and $B$ replaced by $B^n$. Thus,

$$\begin{aligned}
|\epsilon_c^{n+1}(\nu_8) - \epsilon_c(\nu_8)| &= \left|\frac{\epsilon_c^n(\nu_8)[I^n(\nu_8) - B_8^n(P_c)]}{\tilde{I}(\nu_8) + \epsilon_c^n(\nu_8)[I^n(\nu_8) - B_8^n(P_c)] - B_8^n(P_c)} - \frac{I(\nu_8) - \tilde{I}(\nu_8)}{I(\nu_8) - B_8(P_c)}\right| \\
&= \frac{\left|[\epsilon_c^n(\nu_8) - \epsilon_n(\nu_8)] - \epsilon_c^n(\nu_8)\left\{1 - \left[\frac{\tilde{I}(\nu_8) - B_8(P_c)}{\tilde{I}(\nu_8) - B_8^n(P_c)}\right]\left[\frac{I^n(\nu_8) - B_8^n(P_c)}{I(\nu_8) - B_8(P_c)}\right]\right\}\right|}{\left|1 + \epsilon_c^n(\nu_8)\left[\frac{I^n(\nu_8) - B_8^n(P_c)}{\tilde{I}(\nu_8) - B_8^n(P_c)}\right]\right|}.
\end{aligned} \tag{17}$$

In Eq. (17), the apparent temperature profile retrieved without correction for clouds can be assumed to agree with the exact profile above the corresponding cloud top pressure; i.e., $B_8^n(P_c) \approx B_8(P_c)$ (Chahine, 1974). Moreover, since $0 \leqslant \epsilon_c^n(\nu_8) \leqslant 1$, and $0 \leqslant [I^n(\nu_8) - B_8^n(P_c)]/[\tilde{I}(\nu_8) - B_8^n(P_c)]$ if $P_c \leqslant 800$ mb, it can be readily seen that

$$\left|1 + \epsilon_c^n(\nu_8)\left[\frac{I^n(\nu_8) - B_8^n(P_c)}{\tilde{I}(\nu_8) - B_8^n(P_c)}\right]\right| \geqslant 1. \tag{18}$$

Thus, from Eq. (17), we have

$$|\epsilon_c^{n+1}(\nu_8) - \epsilon_c(\nu_8)| \leq \left| [\epsilon_c^n(\nu_8) - \epsilon_c^n(\nu_8)] - \epsilon_c^n(\nu_8) \times \left\{ 1 - \left[ \frac{\tilde{I}(\nu_8) - B_8(P_c)}{\tilde{I}(\nu_8) - B_8^n(P_c)} \right] \left[ \frac{I^n(\nu_8) - B_8^n(P_c)}{I(\nu_8) - B_8(P_c)} \right] \right\} \right| . \quad (19)$$

In Eq. (18), if $I^n(\nu_8) \rightarrow I(\nu_8)$, the last term approaches zero, and the inequality of Eq. (16) is valid.

*c. Discussion of numerical calculations*

The algorithm is numerically carried out by employing the HIRS/2 on board the NOAA 6 and TIROS-N satellites. In the numerical computations, the simulated atmosphere will be divided in such a manner that it coincides with the pressure levels used in the clear column radiance program (CCR) developed at NOAA/NESDIS. There are 40 pressure levels for the CCR program. The program utilizes predetermined transmission profiles which can be empirically adjusted as a function of the known temperature and moisture profiles. The weighting functions of the HIRS channels are depicted in Fig. 1.

In the theoretical analysis, we use the radiosonde profile of Jackson, Mississippi at 1200 (all times GMT), 24 April 1980 as the model atmosphere filled with various types of clouds in an IFOV. The "measured" radiances are simulated for a range of 10 cloud amounts (0.1 to 1.0) and 5 cloud optical thicknesses in the 11 $\mu$m region (1.0 to 5.0). It is very possible that the atmospheric profiles "sensed" by the satellite are different from the radiosonde profiles. Therefore, we introduced a Gaussian random noise distribution into the temperature and water vapor profiles for calculating transmittance profiles and the "measured" radiances. These random noises, which are added to 40 values of temperature and water vapor concentration, are determined by an inverse Gaussian probability distribution function. The standard deviation used for the temperature and water vapor profiles is 1.5 K and 20%, respectively. After this is done, we impose some artificial errors on the "measured" values to simulate instrument noise. The noise is taken to be Gaussian with the zero mean and standard deviations specified for the HIRS channels according to the *NOAA Polar Orbiter Data Users' Guide* (1983). For each cloud amount, optical depth, and cloud top pressure combination, 100 samples are constructed in order to investigate the statistical properties of the retrieval quantities. Results of the retrieved parameters and absolute mean temperature deviation are shown in Figs. 2–7. The figures show the mean value (bias) and fluctuation (standard deviation) of 100 samples for each cloud amount and optical depth combination. First, we assume that the cloud

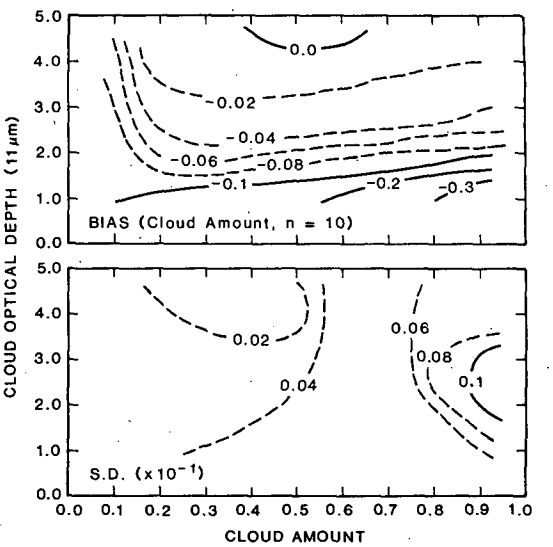


FIG. 3. The bias and standard deviation of computed cloud amounts for various assumed cloud amounts and optical depths.

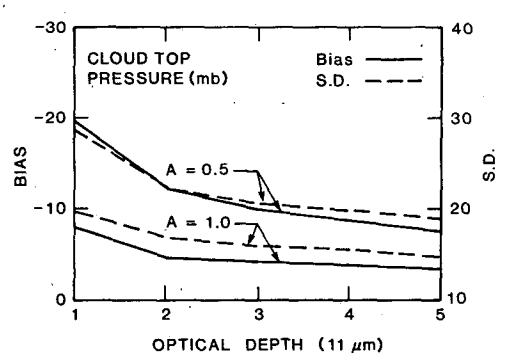


FIG. 2. The bias and standard deviation of computed cloud height (km) for various cloud optical depths with cloud amount equal to 0.5 and 1.0, respectively.

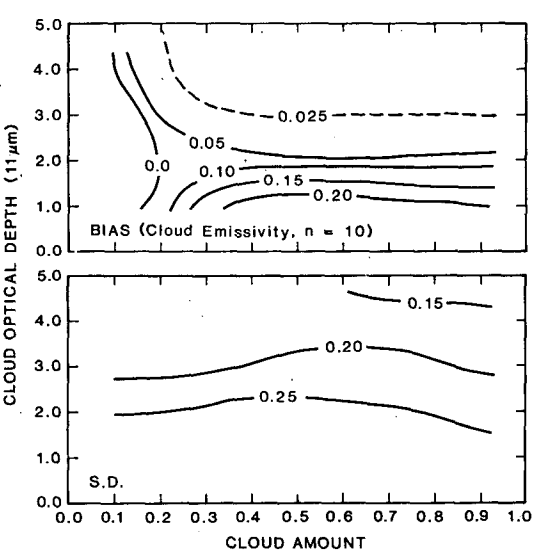


FIG. 4. As in Fig. 3 except for the computed cloud emissivity.

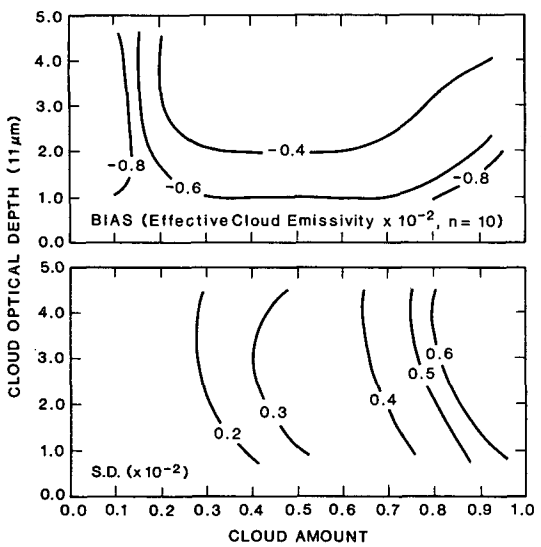


FIG. 5. As in Fig. 3 except for the computed effective cloud emissivity.

top pressure is 300 mb, which is approximately equivalent to 9.37 km for the midlatitude spring climatological profile. Results show that the mean cloud top pressure is generally underestimated. This is particularly evident for optically thin and small fractional clouds (Fig. 2). The uncertainty of the cloud top pressure may propagate and affect the determination of cloud amount and emissivity.

In Figs. 3–7 the results of the retrieved cloud properties are displayed at $n = 10$. As mentioned earlier, the "outer" iteration will stop when the criterion of Eq. (13) is satisfied. However, the iteration usually approaches its asymptotic value after $n = 10$. Beyond this point, iterations do not necessarily extract further information about the cloud parameters and temperature field from the data. In the presence of large noise levels in the measurements, the additional iterations may lead to oscillations in the recovered solutions. In Fig. 3, the mean cloud amounts are estimated so that the results of the entire 100 samples are used for computing the mean values and standard deviation (SD). This means that for cloudy atmospheres that are miscalculated as being clear atmospheres in the algorithm, the results of $A = 0$ will be counted in the estimates of the mean cloud amount and standard deviation (SD). The outcome, as expected, is that the mean cloud amounts for optically thin clouds are underestimated, and the SD also shows that the algorithm is less stable for optically thinner clouds. An underestimation of the cloud amount is also found for the nearly overcast case. This is a result of the constraint we impose, which limits the solution of $A$ to between 0 and 1.

In Fig. 4, the bias and SD of the calculated cloud emissivities are shown. The bias of the cloud emissivity is, in general, opposite to that of the cloud amount. The larger bias and uncertainty of the solutions appear in optically thinner cloud conditions. This is due to the fact that thinner clouds have smaller signatures in the measured data; thus, the measurement noise is more significant in the calculation.

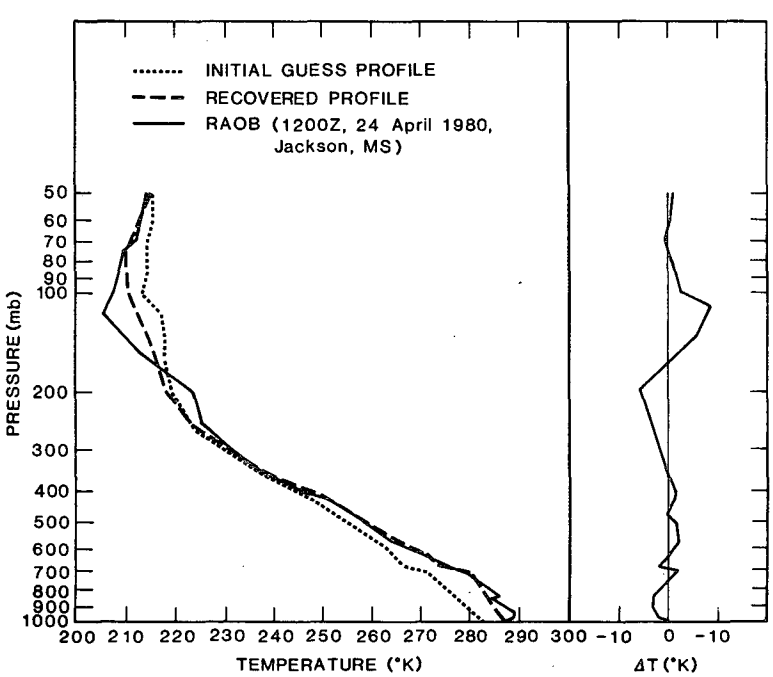


FIG. 6. A randomly selected temperature profile retrieval in a cloudy atmosphere. The RAOB is assumed to be a true solution and the initial guess is a regional climatological profile.

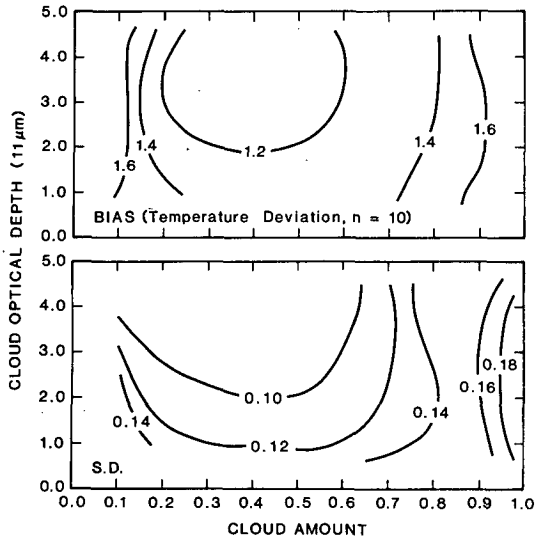


FIG. 7. As in Fig. 3 except for the absolute mean temperature deviation.

The effective cloud emissivity, which is defined in Eq. (6), is an important parameter in the reconstruction of clear radiance. In Fig. 5, the effective cloud emissivity shows a small negative bias overall. The relatively larger bias results from a smaller cloud fractional coverage and thinner clouds. More unstable solutions are shown in cases with larger cloud fractional coverage. This is due to the constraint set up for the calculated cloud amount, as mentioned previously.

For the temperature profile retrieval in cloudy atmospheres, we first display the model temperature profile (1200 24 April 1980, Jackson, MS) and the initial guess profile in Fig. 6. A randomly selected profile retrieved by the algorithm is also shown in the diagram. In general, the retrieved temperature profile agrees with the radiosonde profile except for portions near the tropopause and the temperature inversion close to the ground. From the absolute mean difference of the recovered and radiosonde profiles below 50 mb, one may define the mean temperature deviation $\Delta T_{\text{mean}}$. We then estimate the bias and SD of $\Delta T_{\text{mean}}$ by procedures similar to those for the cloud parameters.

In Fig. 7, the value of $\Delta T_{\text{mean}}$ is shown to be quite consistent with the result of the effective cloud emissivity. However, the bias of $\Delta T_{\text{mean}}$ is generally less dependent on the optical depth than on cloud amount variations. The uncertainty of the temperature retrieval in the case of either a small cloud amount or near overcast is a result of the noise in the calculation of cloud amount, as discussed earlier.

Since the convergence of the effective cloud emissivity directly affects the temperature retrieval, we shall plot the first 10 "outer" iterations as shown in Fig. 8. This figure shows that the bias of the solutions decreases sharply in the first five iterations; the improvement is then much slower in the next five iterations. For different cloud optical depths, thicker clouds appear to have slightly less bias in the calculation of the effective cloud emissivity. However, this is not apparent in temperature retrieval. In Fig. 8, the temperature retrieval for clear atmospheres is also plotted for comparison.

## 4. Applications to the HIRS/2 data of NOAA-6 and TIROS-N satellites

On the basis of the theoretical analysis it appears that a combination of IR sounder data may be utilized to recover the cloud parameters and temperature fields. It is considered desirable and important to apply the developed retrieval scheme to real satellite data. A total number of 30 cases with different synoptic situations were chosen to perform the retrieval exercise. Results will be discussed in this section.

Since NOAA-6 and TIROS-N pass the Great Plains at 1400 and 1000, respectively, the mean value of co-located radiances measured by both satellites may closely represent the observed data at 1200, the time at which the RAOB data are available. The RAOB profiles and surface reports are used in the validation of the computed results.

In this study, we first present cases on 24 April 1980 along with a GOES-East satellite IR picture (Fig. 9)

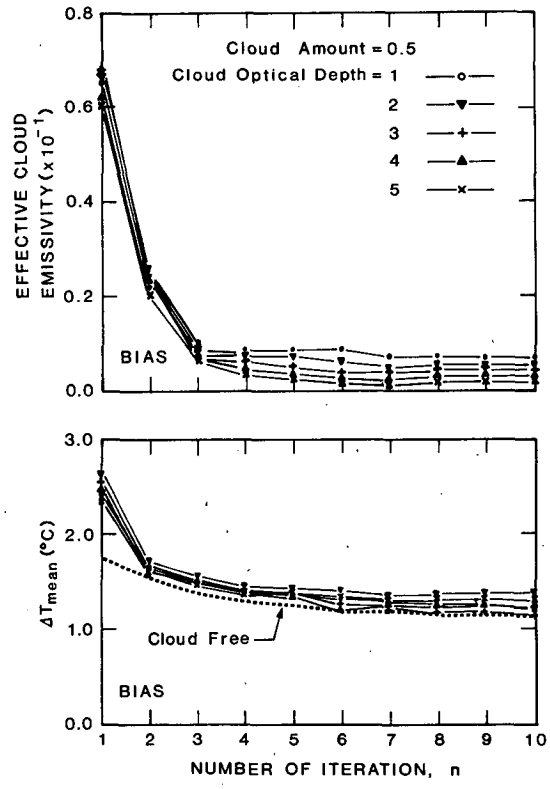


FIG. 8. Rate of convergence of the effective cloud emissivity and absolute mean temperature deviation as judged by the variations of bias with the number of "outer" iterations.

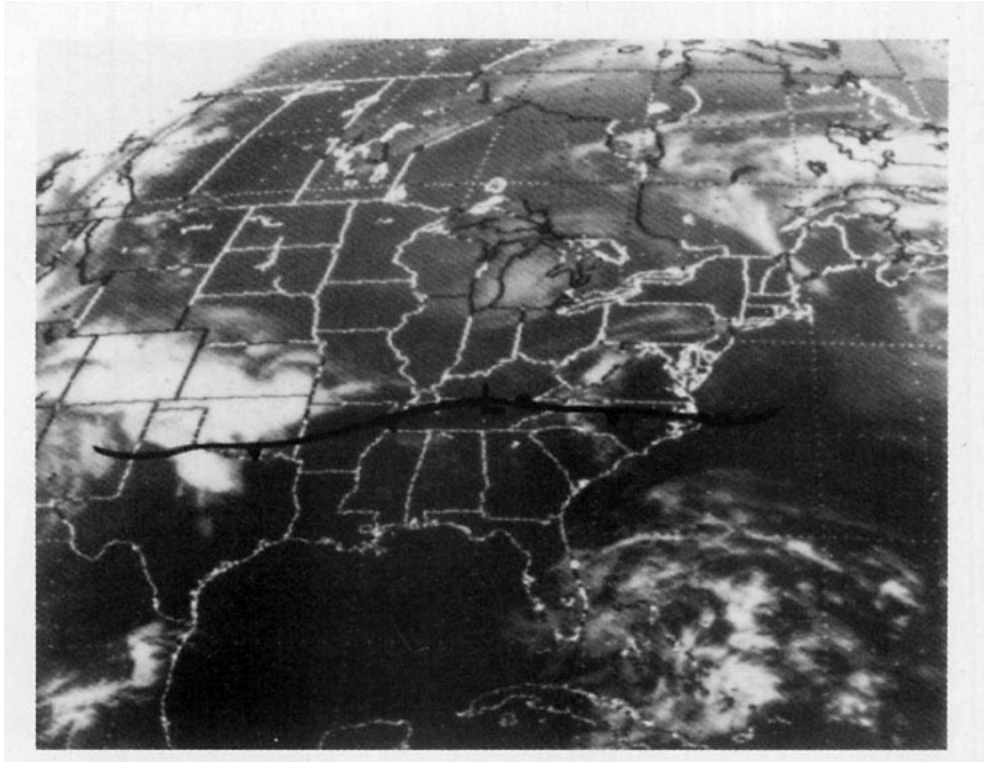

FIG. 9. The GOES IR picture for 1200 GMT 24 April 1980, with the frontal position marked.

and the corresponding synoptic observations (Fig. 10), which show a low pressure area in the eastern Great Plains. A cold front stretched from the center of the low to northern Texas, and a stationary front extended into the Atlantic Ocean. Analyses of the surface reports and the GOES image indicate that cirrus clouds were

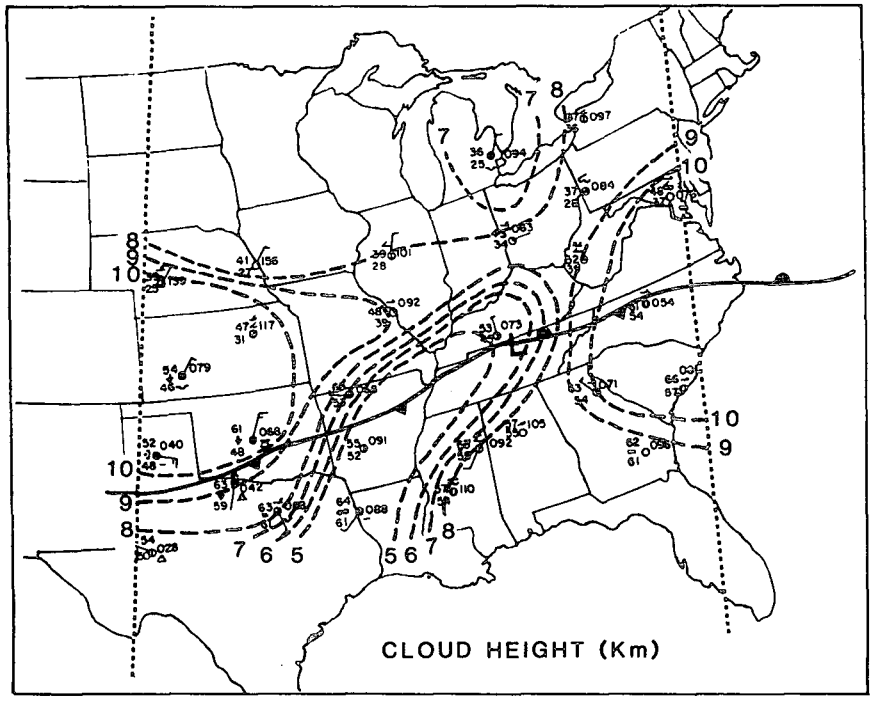


FIG. 10. The synoptic reports of 1200 GMT 24 April 1980, and the mapping of the computed cloud height (km; dashed lines) using HIRS/2 data. The dotted lines indicate the NOAA 6 sub-satellite track.

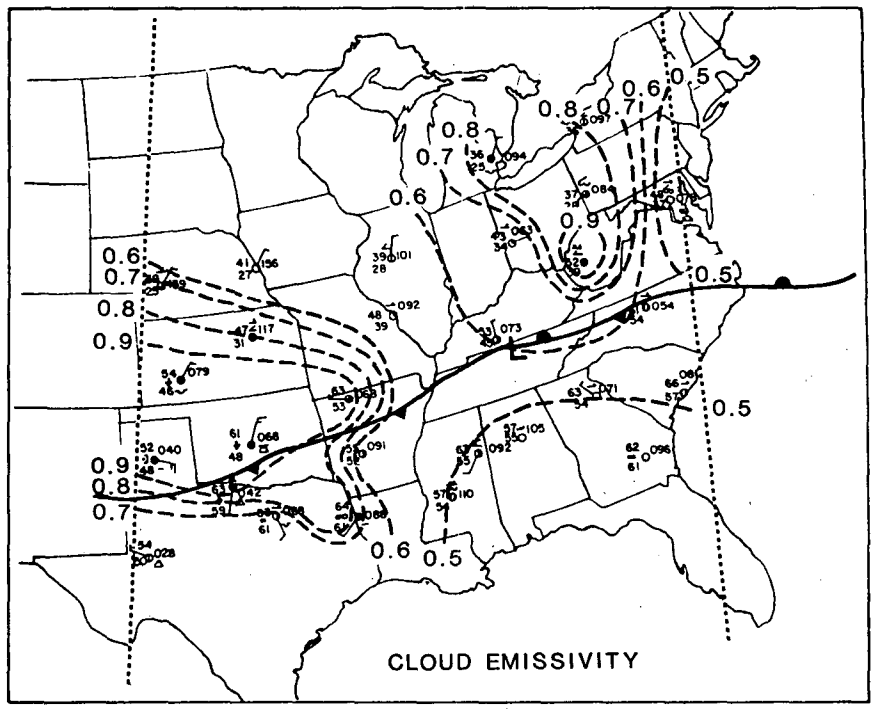


FIG. 11. As in Fig. 10 except for the cloud emissivity.

present in the stationary front area, while multilayer clouds and/or precipitation occurred in the vicinity of the cold front.

Results of the cloud height (which is converted from the cloud top pressure by use of a climatological profile), amount, and emissivity retrieval indicate that an extensive cold system existed over a large portion of Oklahoma and Kansas. The high cloud top height, which was found to be as high as 10 km (Fig. 10), and the high emissivity in this area (Fig. 11) suggest that

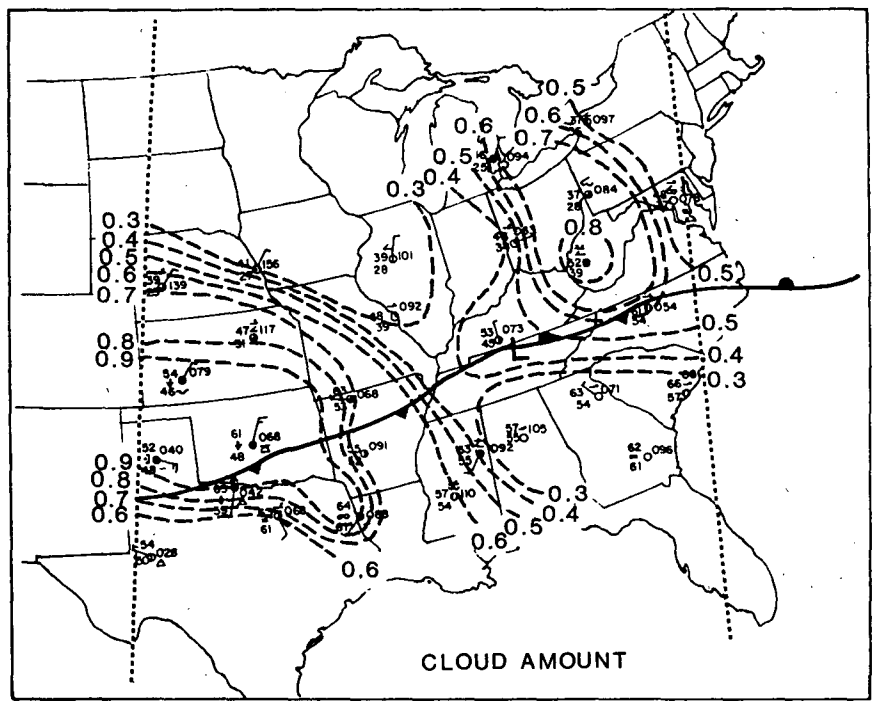


FIG. 12. As in Fig. 10 except for the cloud amount.

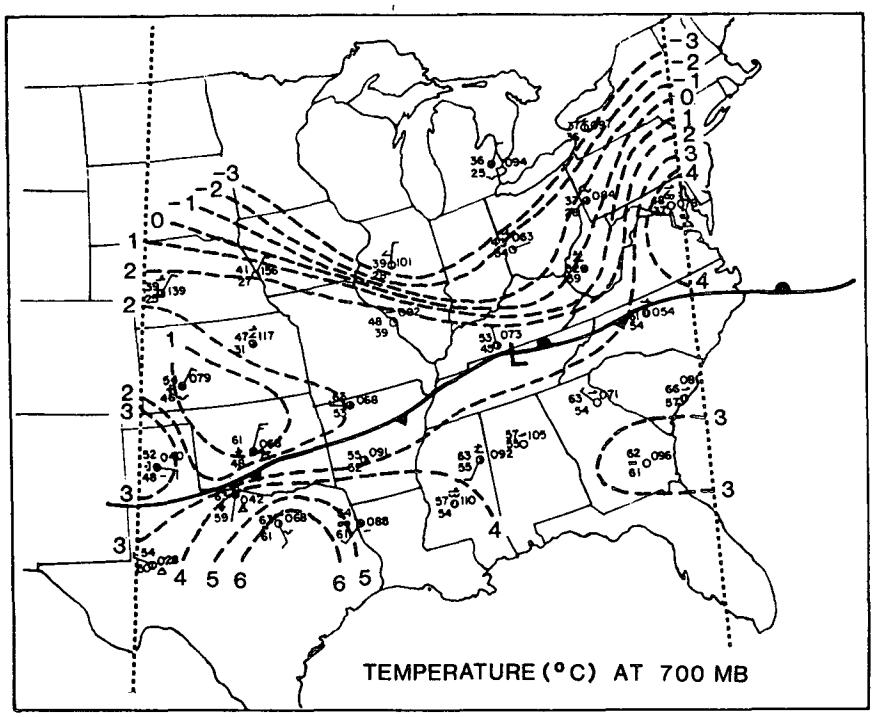


FIG. 13. As in Fig. 10 except for the temperature field at 700 mb.

the system was either composed of thick or multilayer clouds. The cloud amount in this region was close to overcast, as shown in Fig. 12. To the north of the stationary front, extensive cirrus clouds were found. The cloud top heights were at least 9 km, and the emissivities were about 0.6. The cirrus clouds in West Virginia might have had some scattered low clouds underneath them, since a large value of cloud emissivity (>0.8) was found. To the south of the stationary front, the atmosphere was largely clear with only a small fraction

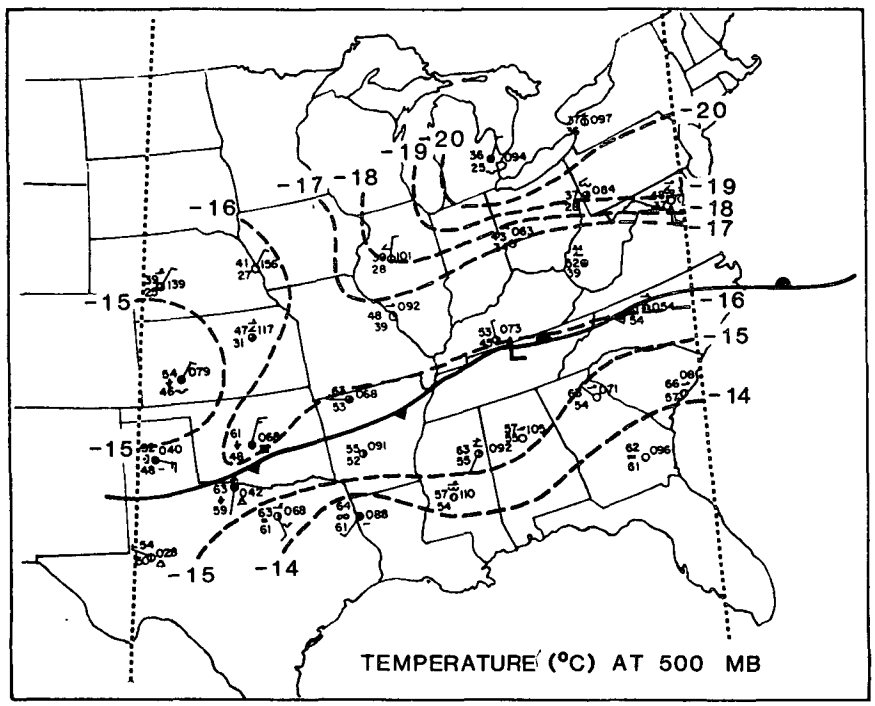


FIG. 14. As in Fig. 13 except for 500 mb.

of high clouds detected. Those high clouds could be thin cirrus because of the small emissivities, as the calculated results show.

For temperature retrieval, we select temperature fields at 700 mb (Fig. 13) and 500 mb (Fig. 14) to display the results, because the cyclonic or sometimes anticyclonic shears are most likely to be present near the 700-mb level, and the jet stream axis is usually located at the 500 mb surface (Palmen and Newton, 1969). At 700 mb, the strong temperature gradients appear to be just north of the stationary front and near the cold front area. This shows the typical crowding of the isotherms in the frontal zone. Figure 14 shows the characteristic baroclinic fields outside the front at the 500 mb level. The temperature distribution is presented along the trough line extending from the Great Lakes area toward Oklahoma.

## 5. Conclusion

In this study, a numerical method for the simultaneous recovery of the cloud top pressure, amount, emissivity, and temperature profile was developed based on parameterized infrared radiative transfer equations for cloudy atmospheres. Theoretical studies were carried out based on synthetic atmospheres containing various thicknesses of fractional cloud cover within an IFOV. It was found that the noise effect is more significant for optically thin clouds and/or small fractional cloud cover in the cloud retrieval. However, the cloud thickness variation has only a slight effect on the temperature retrieval. In general, the resulting cloud parameters retrieved from the present program were found to be reasonably accurate in comparison to theoretically predetermined solutions, and the result of the temperature retrieval in the cloudy cases is within about 0.5°C of that in the clear case, in the sense of absolute mean temperature deviation ($\Delta T_{\text{mean}}$). The initial guess profile plays an important role in the convergence of temperature as well as cloud retrievals.

Numerical experiments were also performed utilizing NOAA-6 and TIROS-N HIRS/2 data in which a mesoscale weather system was analyzed. Results show that the cloud areas were described distinctly in terms of the cloud top height, amount, and emissivity from the program. The temperature fields at the 700 and 500 mb surface also show thermal discontinuity in the frontal zone and the deep trough aloft. The computed cloud amount and temperature field at 700 and 500 mb were qualitatively in good agreement with those obtained from synoptic reports and satellite pictures. However, further verification of the satellite cloud sounding techniques requires carefully designed field experiments such as the First ISCCP Regional Experiment (FIRE, see Schiffer and Rossow, 1983), in which reliable cloud properties, including cloud top height, thickness, and emissivity may be obtained from aircraft observations under the satellite pass.

*Acknowledgments.* This research was supported in part by the CIRA Visiting Members Program under NOAA Grant NA81 RA-00001 and by the Pilot Studies for the International Satellite Cloud Climatology Project under NOAA Contract NA81AA-D-0058. During the final stage of the research work, H. Y. Yeh was supported by the NRC Resident Research Associateship Program at the Goddard Laboratory for Atmosphere.

## REFERENCES

Barcilon, V., 1975: Chahine's relaxation method for the iterative transfer equation. *J. Atmos. Sci.*, **32,** 1626–1630.

Chahine, M. T., 1970: Inverse problems in radiative transfer: Determination of atmospheric parameters. *J. Atmos. Sci.*, **27,** 960–967.

——, 1972: A general relaxation method for inverse solution of the full radiative transfer equation. *J. Atmos. Sci.*, **29,** 741–747.

——, 1974: Remote sounding of cloud atmospheres. I: The single cloud layer. *J. Atmos. Sci.*, **31,** 233–243.

——, 1975: An analytical transformation for remote sensing of clear-column atmospheric temperature profiles. *J. Atmos. Sci.*, **32,** 1946–1952.

——, 1982: Remote sensing of cloud parameters. *J. Atmos. Sci.*, **39,** 159–170.

Feddes, R. G., and K. N. Liou, 1978: Atmospheric ice and water content derived from parameterization of Nimbus 6 high resolution infrared sounder data. *J. Appl. Meteor.*, **17,** 536–551.

Hillger, D. W., and T. H. Vonder Haar, 1977: Deriving mesoscale temperature and moisture fields from satellite radiance measurements over the U.S. *J. Appl. Meteor.*, **16,** 715–726.

——, and ——, 1981: Retrieval and use of high-resolution moisture and stability fields from Nimbus 6 HIRS radiances in preconvective situations. *Mon. Wea. Rev.*, **109,** 1788–1806.

Hunt, G. E., 1973: Radiative properties of terrestrial clouds at visible and infrared thermal window wavelengths. *Quart. J. Roy. Meteor. Soc.*, **99,** 346–369.

Liou, K. N., 1980: *An Introduction to Atmospheric Radiation,* Academic Press, 404 pp.

McCleese, D. J., and L. S. Wilson, 1976: Cloud top height from temperature sounding instruments. *Quart. J. Roy. Meteor. Soc.*, **102,** 781–790.

NOAA, 1983: *NOAA Polar Orbiter Data (TIROS-N, NOAA-6, NOAA-7, NOAA-8) Users' Guide.* K. B. Kidwell, Ed., NOAA/NESDIS, National Climate Data Center, Satellite Data Service Division, World Weather Building, Washington, DC.

Palmen, E., and C. W. Newton, 1969: *Atmospheric Circulation Systems: Their Structure and Physical Interpretation,* Academic Press.

Paltridge, G. W., and C. M. R. Platt, 1976: *Radiative Processes in Meteorology and Climatology,* Elsevier.

Schiffer, R. A., and W. B. Rossow, 1983: The International Satellite Cloud Climatology Project (ISCCP): The first project of the World Climate Research Programme. *Bull. Amer. Meteor. Soc.*, **64,** 779–784.

Smith, W. L., 1970: Iterative solution of the radiative transfer equation for the temperature and absorbing gas profile of an atmosphere. *Appl. Opt.*, **9,** 1993–1999.

——, H. M. Woolf, C. M. Hayden, D. Q. Wark and L. M. McMillin, 1979: The TIROS-N Operational Vertical Sounder. *Bull. Amer. Meteor. Soc.*, **60,** 117–118.

Susskind, J., J. Rosenfield and D. Reuter, 1984: Remote sensing of weather and climate parameters from HIRS2/MSU on TIROS-N. *J. Geophys. Res.*, **89,** 4677–4697.

Wielicki, B. A., and J. A. Coakley, Jr., 1981: Cloud retrieval using infrared sounder data: Error analysis. *J. Appl. Meteor.*, **20,** 157–169.

Yeh, H. Y., and K. N. Liou, 1983: Satellite remote sounding cloud parameters by infrared and microwave data. *J. Climate Appl. Meteor.*, **22,** 201–213.

——, 1984: Determination of cloud parameters from infrared sounder data. *J. Geophys. Res.*, **89,** 11,759–11,770.